

Article

# Microstructure, Mechanical and Corrosion Behaviors of CoCrFeNiAl<sub>0.3</sub> High Entropy Alloy (HEA) Films

Libo Gao <sup>1,2</sup> , Weibing Liao <sup>1,3</sup> , Hongti Zhang <sup>1,2</sup>, James Utama Surjadi <sup>1</sup>, Dong Sun <sup>1</sup> and Yang Lu <sup>1,2,\*</sup> 

<sup>1</sup> Department of Mechanical and Biomedical Engineering, City University of Hong Kong, Hong Kong; bogao5-c@my.cityu.edu.hk (L.G.); liaowb@szu.edu.cn (W.L.); hozhang7@cityu.edu.hk (H.Z.); jusurjadi2-c@my.cityu.edu.hk (J.U.S.); medsun@cityu.edu.hk (D.S.)

<sup>2</sup> Shenzhen Research Institute, City University of Hong Kong, Shenzhen 518057, China

<sup>3</sup> College of Physics and Energy, Shenzhen University, Shenzhen 518060, China

\* Correspondence: yanglu@cityu.edu.hk; Tel.: +852-3442-4061

Received: 30 July 2017; Accepted: 22 September 2017; Published: 26 September 2017

**Abstract:** The HEA-CoCrFeNiAl<sub>0.3</sub> thin film in this study has been successfully developed by radio frequency (RF) magnetron sputtering to meet the increasing demand in engineering applications. Its microstructure and surface profile were investigated accordingly. The as-synthesized HEA film was found to have a homogeneous element distribution and ultra-smooth surface, exhibiting a typical face-centered cubic (FCC) solid solution. The film showed better mechanical properties than its bulk counterpart, with a Young's modulus and hardness of ~201.4 GPa and ~11.5 GPa, respectively. Furthermore, corrosion tests demonstrated decreased sensitivity to localized corrosion in comparison to the commercial 304 stainless steel in NaCl solution.

**Keywords:** high entropy alloy; coating; sputtering; mechanical behavior; corrosion resistance

## 1. Introduction

High-entropy alloys (HEA) have been of great interest recently, based on their unique alloy-design concept. Prominent advantages that have been explored include increased strength and hardness [1,2], excellent thermal stability [3], great fatigue, and superior wear and corrosion resistances [4–6]. This is primarily derived from the ability of the elements to stabilize as a single-phase crystalline structure [7,8].

As a typical case in point, CoCrFeNiAl<sub>x</sub> family HEA has aroused much attention to date due to its unique properties in terms of its balanced combination of high tensile strength and ductility at ambient or cryogenic temperatures [9,10]. It also exhibits versatile microstructures and other interesting properties compared to conventional alloy systems [2,6,11–13]. However, the CoCrFeNiAl<sub>x</sub> HEA fabricated using the conventional vacuum arc melting methodology is always in the bulk solid form. This would be costly, impeding its practicability for real-life applications [2,9,14,15]. Alternatively, it is widely known that thin films can be used as a protective and mechanically enhancing surface coating on the substrate [16–20]. Therefore, incorporating HEA as a thin film material would tremendously extend the scope of its practical application. Among the methods for fabricating HEA films, sputtering is the most widely used because of its fast and efficient fabrication procedure [21,22]. For instance, AlCoCrCu<sub>0.5</sub>NiFe [23], AlCoCrCuFeNi [24], and CoCrFeCuNi HEA films [25] have previously been fabricated through sputtering, and their mechanical properties have been investigated. However, the mechanical characterizations of CoCrFeNiAl<sub>x</sub> film fabricated using the sputtering method has been little reported. In addition to its mechanical properties, corrosion-resistance is another important factor that needs to be considered for practical applications of HEA. Thus, this has also been extensively studied [26–28]. Nevertheless, the corrosion performance of HEA coatings synthesized via sputtering has not yet been widely reported.

In this study, the HEA ( $\text{CoCrFeNiAl}_{0.3}$ ) thin film was successfully fabricated via the radio frequency (RF) sputtering technique with the as-cast bulk target serving as the element source. Subsequently, a series of characterization methods, including X-ray diffraction (XRD) and transmission electron microscopy (TEM), were employed to precisely verify its crystalline microstructure. In addition, scanning electron microscopy (SEM) and white light interferometry (WLI) were used to investigate the microstructure and surface roughness of the fabricated HEA film. Finally, the mechanical and corrosion tests of the HEA film were also explored.

## 2. Materials and Methods

As shown in Figure 1a, reactive high-vacuum RF magnetron sputtering was employed to fabricate high-entropy  $\text{CoCrFeNiAl}_{0.3}$  alloy thin films on silicon substrates. The target with a composition of  $\text{CoCrFeNiAl}_{0.3}$  was prepared by metallurgy with high purity (>99.99%) raw materials of cobalt, chromium, iron, nickel, and aluminum. Prior to sputtering, the target was initially cleaned by argon ion bombardment for at least 2 min to remove any oxide and other possible contaminants. The Si substrate was also cleaned ultrasonically for 15 min, followed by rinsing with acetone, ethanol and deionized water. The rotation speed of the substrate was set to 2 rpm to guarantee homogeneous deposition. High purity argon was introduced into the vacuum chamber once the base pressure was below  $1.0 \times 10^{-6}$  Pa. The ignition argon flow was set to 22 standard cubic centimeters per minute (sccm). The film was deposited on the silicon wafer at room temperature for 3 h, and the argon flow rate was fixed at 12 sccm with a working distance of about 80 mm and a working pressure of about 0.69 Pa. The deposition power was controlled at 500 W. Thin films of different thickness can be obtained by controlling the deposition time.

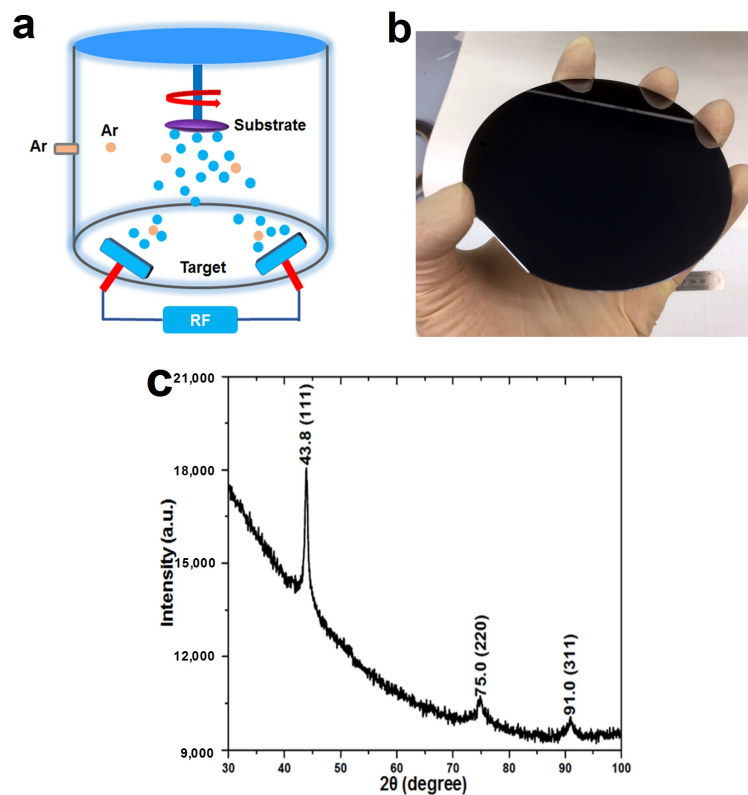


**Figure 1.** (a) The schematic illustration of fabrication the HEA film; (b) The digital optical images of the HEA film on Si substrate; (c) XRD of the HEA film.

The microstructures and the chemical deposition of the as-deposited films were characterized using SEM (Quanta 450, FEI, Hillsboro, OR, USA) equipped with an energy dispersive X-ray

spectrometer (EDX, Oxford Instruments, Oxford, UK) operated at 20 kV. The surface roughness was characterized by WLI using Wyko NT9300 Surface Profiler (Bruker, Billerica, MA, USA). XRD was used to characterize the phase structure of the as-deposited films. The modulus and hardness of the as-deposited film were measured using nanoindentation with a Berkovich triangular pyramid indenter. The maximum load into the sample surface was 500  $\mu$ N. The microstructure of the thin film was examined by high-resolution TEM (HRTEM, JEM-2100F, JEOL, Tokyo, Japan) operated at 200 kV.

The potentiodynamic polarization experiments were performed on Chenhua CHI 760E electrochemical working station (Chenhua, Shanghai, China). A typical three-electrode measurement system was implemented using 3.5 wt % NaCl solution at room temperature. Either the HEA or 304 stainless steel was regarded as the working electrode, with a platinum foil as the counter electrode, and a saturated calomel electrode (SCE) as the reference electrode. Note that the open current potential (OCP) was recorded for 1 h to sustain a stable potential before the potentiodynamic polarization. The test was conducted at a scan rate of  $1 \text{ mV}\cdot\text{s}^{-1}$  from  $-1$  to  $1.5$  V. To certify the data reproducibility, the test was repeated 5 times.

### 3. Results and Discussion

Figure 1 exhibits the fabrication procedure and corresponding phase characterization of the HEA film. A reasonably smooth surface can be seen in Figure 1b, showing homogenous deposition of the HEA film on Si substrate macroscopically. XRD was employed to identify the primary phase structure, as shown in Figure 1c. Obvious (111), (220) and (311) phase peaks were observed, corresponding to a typical FCC crystal structure for the HEA film. This is in accordance with a previous report on a HEA with the same constituents [14]. Therefore, it can be concluded that the sputtered HEA film is fundamentally a typical FCC solid solution structure.

WLI was used to obtain the roughness and surface profiles of the synthesized HEA film. This is shown in Figure 2a–c. The mean roughness ( $R_a$ ) value of the HEA film is only 0.89 nm, indicating a smooth surface morphology. The thickness of the HEA deposited for 3 h is approximately 3.3  $\mu$ m through the cross-section SEM image as shown in Figure 2d. Additionally, no obvious voids or cracks were observed, although there is a large quantity of fine-sized precipitates in the enlarged view of the SEM image in Figure 2e.

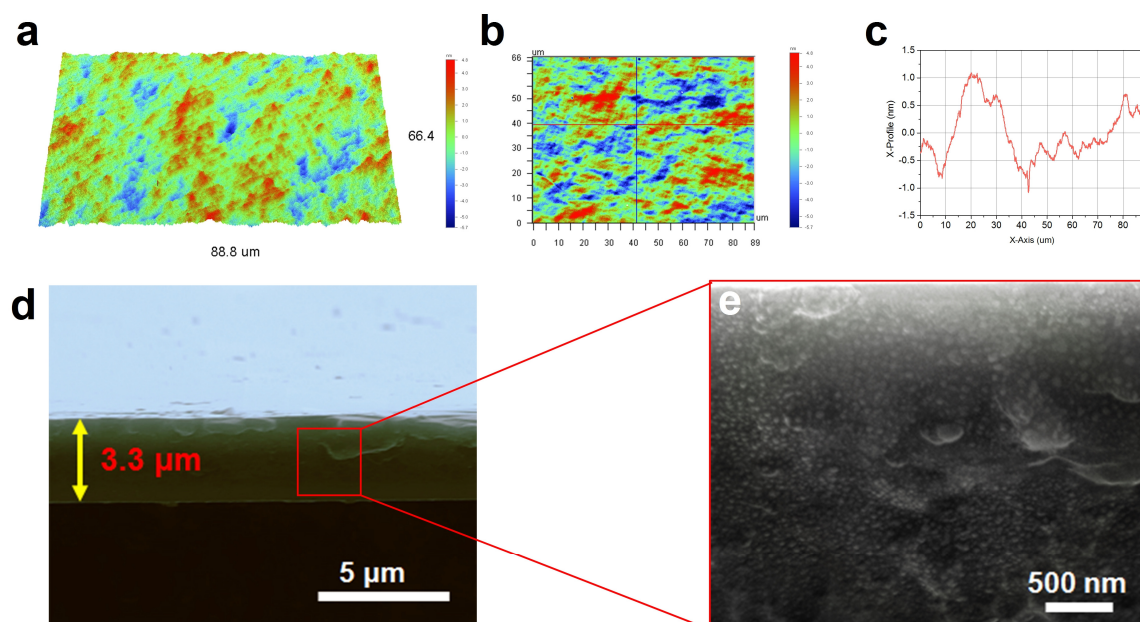


**Figure 2.** (a–c) 3D and 2D surface profiles of the synthesized HEA film characterized by WLI technique; (d–e) Cross-section view of the HEA film.

In order to analyze the chemical composition of the HEA film, SEM–EDX mapping was implemented. As anticipated, and shown in Figure 3, there is a uniform distribution of the five elements, with no other elements found on the surface of the HEA film. Importantly, the atomic concentration of the elements is very close to 1:1:1:1:0.3, which is nearly the same with its bulk counterpart. This indicates that the sputtering technique is an effective route to deposit high-quality HEA films, which may have the potential to be used for high temperature applications [14].

TEM was employed to have a deep observation of the micro-morphology and phase structure of the HEA film. Figure 4a shows the columnar grains corresponding to the numerous precipitates present in the thin film, with no observable voids or cracks. The columnar growth direction is perpendicular to the surface of substrate due to the sputtering process. This behavior is similar to other reports [29]. Additionally, the precipitates would enhance the hardness because of the dislocation by-pass and particle-shearing principle. The inset shows the corresponding selected area electron diffraction (SAED) patterns exhibiting a typical polycrystalline structure, which is in good agreement with the XRD results. Figure 4b indicates that the average grain size is about 10 nm, which is supposed to be beneficial for enhancing the mechanical property of the HEA film considering the “the smaller, the stronger” effect [30]. Specifically, as shown in Figure S1, the TEM–EDX spot analysis indicates that the nano-sized precipitates in the CoCrFeNiAl<sub>0.3</sub> alloy show less averaged content of Al element than other regions. Also, combining the TEM result with that of the XRD, it was supposed that the as-synthesized HEA film is a polycrystalline solid solution.

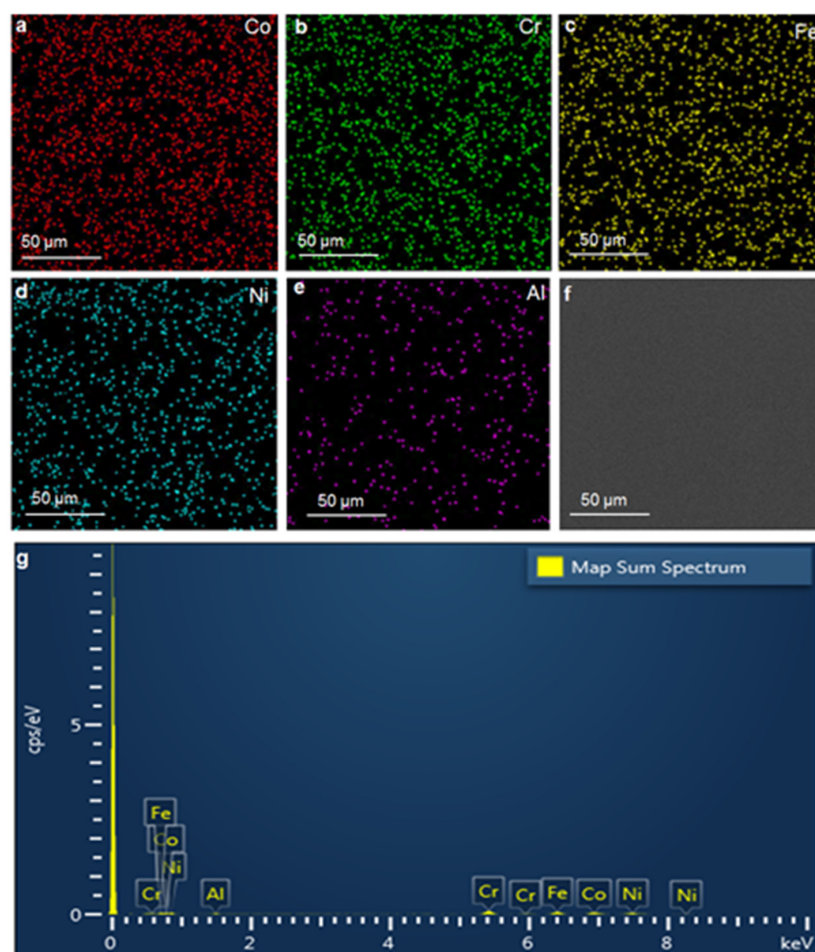


**Figure 3.** SEM–EDS mapping and typical SEM images of the HEA film, indicating the homogeneous element distribution: (a) Co element; (b) Cr element; (c) Fe element; (d) Ni element; (e) Al element; (f) Corresponding original SEM image; (g) The chemical compositions of the HEA film.

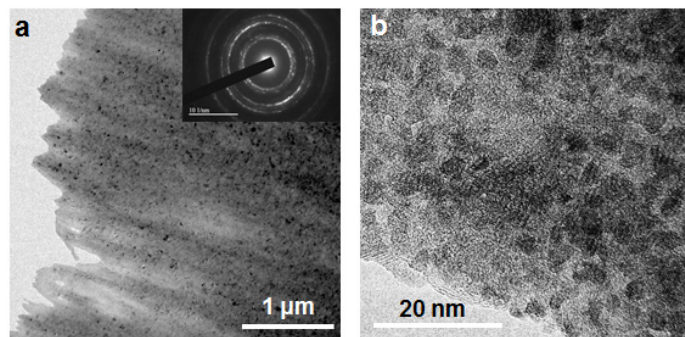


**Figure 4.** (a) TEM and (b) HRTEM images of the HEA film, suggesting its polycrystalline structures.

Figure 5a shows the nano-indentation test results of the HEA film. The average Young's modulus and hardness of the HEA film are approximately 201.4 GPa and 11.5 GPa, respectively. Importantly, the hardness value obtained exceeds the similar as-cast bulk HEA ( $\text{CoCrFeNiAl}_{0.3}$ ) by 3.5–4 times [14]. Typically, strength is directly proportional to hardness, thus the high hardness value obtained implies the possible high strength of the HEA film [31]. This enhanced hardness is mainly ascribed to the shearing mechanism of dislocated particles or by-pass mechanism (Orowan-type), which induces the hardening produced by the precipitates observed in Figures 2 and 4 [9].

High corrosion resistance is crucial for the practical application of HEA film. In this regard, the corrosion tests were employed in 3.5 wt % NaCl solution at room temperature. As shown in Figure 5b and Table 1, the corrosion potential ( $E_{\text{corr}}$ ) for HEA is slightly higher than that of 304 stainless steel, while the corrosion density ( $I_{\text{corr}}$ ) is marginally smaller. The critical pitting potential ( $E_p$ ) refers to the potential value at which the current density suddenly increases, indicating that the protective passive film has started to pit. The  $E_p$  of 304 stainless steel is inferior to that of the HEA, and the passive zone is much larger, which demonstrates that the passive HEA film coating has better resistance to localized corrosion. This behavior is, on one hand, due to the relatively small-sized distributed homogeneous nanoparticles which can easily form a dense oxide layer that serves as a passive protective film. Additionally, the elements Co, Cr and Ni in HEA have excellent corrosion resistance, and the protective layer is capable of easily being built on the surface of the coating [32]. On the other hand, the characteristic homogeneous distribution of elements in the HEA film, which is coherent with the bulk sample, is another important factor.

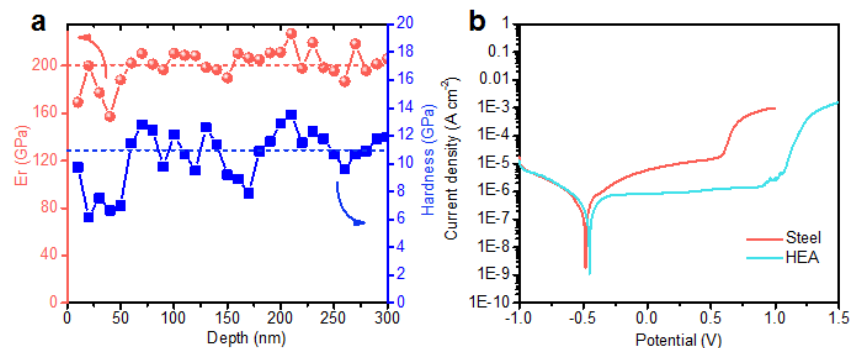


**Figure 5.** (a) Mechanical and (b) corrosion tests of the HEA film and steel in 3.5 wt % NaCl solution.

**Table 1.** Electrochemical parameters of HEA and 304 stainless steel in 3.5 wt % NaCl solution.

Sample	$E_{\text{corr}}$ (V <sub>SCE</sub> )	$I_{\text{corr}}$ ( $\mu\text{A cm}^{-2}$ )	$E_p$ (V <sub>SCE</sub> )
HEA	-0.451	0.103	1.07
Steel	-0.482	0.125	0.6

#### 4. Conclusions

In summary, CoCrFeNiAl<sub>0.3</sub> thin film was successfully fabricated using the RF sputtering technique. The phase structure was confirmed by XRD and TEM to be a polycrystalline structure consisting of simple FCC structures. Additionally, the HEA film was shown to have a homogeneous element distribution and smooth surface with a mean roughness less than 1 nm. The nano-indentation test results demonstrate the excellent mechanical properties of the HEA, with a high Young's modulus (201.4 GPa) and hardness (11.5 GPa), outperforming its bulk counterpart. The potentiodynamic polarization test in 3.5 wt % NaCl demonstrates that the HEA coating shows better corrosion resistance to localized corrosion than 304 stainless steel at room temperature, which is primarily due to the homogeneously distributed elements forming the protective layer.

**Supplementary Materials:** The following are available online at <http://www.mdpi.com/2079-6412/7/10/156/s1>. Figure S1: TEM–EDS for the HEA film.

**Acknowledgments:** The authors gratefully thank the funding support from Shenzhen Science and Technology Innovation Committee under the grants JCYJ20160401100358589. D.S. acknowledges the funding from RGC under the project GRF CityU1211714.

**Author Contributions:** Yang Lu designed the project. Libo Gao conducted the major experiments, analyzed the data, and wrote the manuscript. Weibing Liao contributed to the film deposition method. Hongti Zhang performed the TEM experiments. James Utama Surjadi analyzed the data and partially wrote the manuscript. All authors have given approval to the final version of the paper.

**Conflicts of Interest:** The authors report no conflict of interest.

#### References

1. Zhou, Y.; Zhang, Y.; Wang, Y.; Chen, G. Solid solution alloys of properties Solid solution alloys of AlCoCrFeNiTi<sub>x</sub> with excellent room-temperature. *Appl. Phys. Lett.* **2014**, *90*, 181904. [[CrossRef](#)]
2. Ma, S.G.; Zhang, Y. Effect of Nb addition on the microstructure and properties of AlCoCrFeNi high-entropy alloy. *Mater. Sci. Eng. A* **2012**, *532*, 480–486. [[CrossRef](#)]
3. Zou, Y.; Ma, H.; Spolenak, R. Ultrastrong ductile and stable high-entropy alloys at small scales. *Nat. Commun.* **2015**, *6*, 7748. [[CrossRef](#)] [[PubMed](#)]
4. Chuang, M.; Tsai, M.; Wang, W.; Lin, S.; Yeh, J. Microstructure and wear behavior of Al<sub>x</sub>Co<sub>1.5</sub>CrFeNi<sub>1.5</sub>Ti<sub>y</sub> high-entropy alloys. *Acta Mater.* **2011**, *59*, 6308–6317. [[CrossRef](#)]
5. Hemphill, M.A.; Yuan, T.; Wang, G.Y.; Yeh, J.W.; Tsai, C.W.; Chuang, A.; Liaw, P.K. Fatigue behavior of Al<sub>0.5</sub>CoCrCuFeNi high entropy alloys. *Acta Mater.* **2012**, *60*, 5723–5734. [[CrossRef](#)]
6. Cocrfeni, A.; Lin, C.; Tsai, H. Intermetallics evolution of microstructure, hardness, and corrosion properties of high-entropy. *Intermetallics* **2011**, *19*, 288–294.
7. Gludovatz, B.; Hohenwarter, A.; Catoor, D.; Chang, E.H.; George, E.P.; Ritchie, R.O. A fracture-resistant high-entropy alloy for cryogenic applications. *Science* **2014**, *345*, 1153–1158. [[CrossRef](#)] [[PubMed](#)]
8. Yeh, J.W.; Chen, S.K.; Lin, S.J.; Gan, J.Y.; Chin, T.S.; Shun, T.T.; Tsau, C.H.; Chang, S.Y. Nanostructured high-entropy alloys with multiple principal elements: Novel alloy design concepts and outcomes. *Adv. Eng. Mater.* **2004**, *6*, 299–303. [[CrossRef](#)]
9. Li, D.; Li, C.; Feng, T.; Zhang, Y.; Sha, G.; Lewandowski, J.J.; Liaw, P.K.; Zhang, Y. High-entropy Al<sub>0.3</sub>CoCrFeNi alloy fibers with high tensile strength and ductility at ambient and cryogenic temperatures. *Acta Mater.* **2017**, *123*, 285–294. [[CrossRef](#)]
10. Ma, S.; Zhang, S.; Gao, M.C.; Liaw, P.K.; Zhang, Y. A successful synthesis of the CoCrFeNiAl<sub>0.3</sub> single-crystal, high-entropy alloy by Bridgman solidification. *JOM* **2013**, *65*, 1751–1758. [[CrossRef](#)]
11. Zhu, Z.G.; Sun, Y.F.; Goh, M.H.; Ng, F.L.; Nguyen, Q.B.; Fujii, H.; Nai, S.M.L.; Wei, J.; Shek, C.H. Friction stir welding of a CoCrFeNiAl<sub>0.3</sub> high entropy alloy. *Mater. Lett.* **2017**, *205*, 142–144. [[CrossRef](#)]
12. Wang, Y.; Li, B.; Ren, M.; Yang, C.; Fu, H. Microstructure and compressive properties of AlCrFeCoNi high entropy alloy. *Mater. Sci. Eng. A* **2008**, *491*, 154–158. [[CrossRef](#)]
13. Kao, Y.; Chen, S.; Chen, T.; Chu, P.; Yeh, J.; Lin, S. Electrical, magnetic, and Hall properties of Al<sub>x</sub>CoCrFeNi high-entropy alloys. *J. Alloys Compd.* **2011**, *509*, 1607–1614. [[CrossRef](#)]

14. Ma, S.; Zhang, S.; Qiao, J.; Wang, Z.; Gao, M.C.; Jiao, Z.; Yang, H.; Zhang, Y. Superior high tensile elongation of a single-crystal CoCrFeNiAl<sub>0.3</sub> high-entropy alloy by Bridgman solidification. *Intermetallics* **2014**, *54*, 104–109. [[CrossRef](#)]
15. Shi, Y.; Yang, B.; Liaw, P. Corrosion-resistant high-entropy alloys: A review. *Metals* **2017**, *7*, 43. [[CrossRef](#)]
16. Jia, H.; Liu, F.; An, Z.; Li, W.; Wang, G.; Chu, J.P.; Jang, J.S.C.; Gao, Y.; Liaw, P.K. Thin-film metallic glasses for substrate fatigue-property improvements. *Thin Solid Films* **2014**, *561*, 2–27. [[CrossRef](#)]
17. Chu, J.P.; Greene, J.E.; Jang, J.S.C.; Huang, J.C.; Shen, Y.L.; Liaw, P.K.; Yokoyama, Y.; Inoue, A.; Nieh, T.G. Bendable bulk metallic glass: Effects of a thin, adhesive, strong, and ductile coating. *Acta Mater.* **2012**, *60*, 3226–3238. [[CrossRef](#)]
18. Chu, J.P.; Liu, T.Y.; Li, C.L.; Wang, C.H.; Jang, J.S.C.; Chen, M.J.; Chang, S.H.; Huang, W.C. Fabrication and characterizations of thin film metallic glasses: Antibacterial property and durability study for medical application. *Thin Solid Films* **2014**, *561*, 102–107. [[CrossRef](#)]
19. Zhang, H.; Pan, Y.; He, Y.; Jiao, H. Microstructure and properties of 6FeNiCoSiCrAlTi high-entropy alloy coating prepared by laser cladding. *Appl. Surf. Sci.* **2011**, *257*, 2259–2263. [[CrossRef](#)]
20. Luo, S.; Lee, J.H.; Liu, C.W.; Shieh, J.M.; Shen, C.H.; Wu, T.T.; Jang, D.; Greer, J.R. Strength, stiffness, and microstructure of Cu(In,Ga)Se<sub>2</sub> thin films deposited via sputtering and co-evaporation. *Appl. Phys. Lett.* **2014**, *105*, 011907. [[CrossRef](#)]
21. Dou, D.; Li, X.C.; Zheng, Z.Y.; Li, J.C. Coatings of FeAlCoCuNiV high entropy alloy. *Surf. Eng.* **2016**, *32*, 766–770. [[CrossRef](#)]
22. Li, X.; Zheng, Z.; Dou, D.; Li, J.; Centre, E.T. Microstructure and properties of coating of FeAlCuCrCoMn high entropy alloy deposited by direct current magnetron sputtering. *Mater. Res.* **2016**, *19*, 802–806. [[CrossRef](#)]
23. Huang, Y.S.; Chen, L.; Lui, H.W.; Cai, M.H.; Yeh, J.W. Microstructure, hardness, resistivity and thermal stability of sputtered oxide films of AlCoCrCu<sub>0.5</sub>NiFe high-entropy alloy. *Mater. Sci. Eng. A* **2007**, *457*, 77–83. [[CrossRef](#)]
24. Braeckman, B.R.; Boydens, F.; Hidalgo, H.; Dutheil, P.; Jullien, M.; Thomann, A.-L.; Depla, D. High entropy alloy thin films deposited by magnetron sputtering of powder targets. *Thin Solid Films* **2015**, *580*, 71–76. [[CrossRef](#)]
25. Ma, Y.; Peng, G.J.; Wen, D.H.; Zhang, T.H. Nanoindentation creep behavior in a CoCrFeCuNi high-entropy alloy film with two different structure states. *Mater. Sci. Eng. A* **2015**, *621*, 111–117. [[CrossRef](#)]
26. Chen, Y.Y.; Duval, T.; Hung, U.D.; Yeh, J.W.; Shih, H.C. Microstructure and electrochemical properties of high entropy alloys—a comparison with type-304 stainless steel. *Corros. Sci.* **2005**, *47*, 2257–2279. [[CrossRef](#)]
27. Tang, Z.; Huang, L.; He, W.; Liaw, P.K. Alloying and processing effects on the aqueous corrosion behavior of high-entropy alloys. *Entropy* **2014**, *16*, 895–911. [[CrossRef](#)]
28. Qiu, Y.; Gibson, M.A.; Fraser, H.L.; Birbilis, N. Corrosion characteristics of high entropy alloys. *Mater. Sci. Technol.* **2015**, *31*, 1235–1243. [[CrossRef](#)]
29. An, Z.; Jia, H.; Wu, Y.; Rack, P.D.; Patchen, A.D.; Liu, Y.; Ren, Y.; Li, N.; Liaw, P.K. Solid-solution CrCoCuFeNi high-entropy alloy thin films synthesized by sputter deposition. *Mater. Res. Lett.* **2015**, *3*, 203–209. [[CrossRef](#)]
30. Blanco, A.; Chomski, E.; Grabtchak, S.; Marta, I.; John, S.; Leonard, S.W.; Cefe, L.; Francisco, M.; Hernan, M.; Mondia, J.P.; et al. Large-scale synthesis of a silicon photonic crystal with a complete three-dimensional bandgap. *Nature* **2000**, *405*, 437–440. [[PubMed](#)]
31. Zhang, P.; Li, S.; Zhang, Z. General relationship between strength and hardness. *Mater. Sci. Eng. A* **2011**, *529*, 62–73. [[CrossRef](#)]
32. Gan, Y.; Wang, W.; Guan, Z.; Cui, Z. Multi-layer laser solid forming of Zr<sub>65</sub>Al<sub>7.5</sub>Ni<sub>10</sub>Cu<sub>17.5</sub> amorphous coating: Microstructure and corrosion resistance. *Opt. Laser Technol.* **2015**, *69*, 17–22. [[CrossRef](#)]



© 2017 by the authors. Licensee MDPI, Basel, Switzerland. This article is an open access article distributed under the terms and conditions of the Creative Commons Attribution (CC BY) license (<http://creativecommons.org/licenses/by/4.0/>).